UNIVERSITÀ DEGLI STUDI DI
MILANO-BICOCCA

Scuola di Scienze Matematiche Fisiche e Naturali
Corso di laurea Triennale in Fisica

PROBING OPTICAL AND RADIO-LOUD AGN FRACTIONS : A COMPARATIVE ANALYSIS BETWEEN BCGs AND NON-BCGs SAMPLES at z < 0.1

Candidate:
Andrea Maccarinelli

Supervisor:
Prof. Sebastiano Cantalupo

Co-supervisors:
Dott. Andrea Travascio

anno accademico 2022/2023

Abstract

Brightest cluster galaxies (BCGs) are the most massive and luminous galaxies located near the center of relaxed, virialized, and undisturbed galaxy clusters in the local Universe ([1, 2]). According to several observational studies ([3, 4]), these objects experience a special formation process differing from general galaxy evolution.

Current theoretical models (e.g., [5, 6]) predict that dry mergers are the dominant mechanisms responsible for their mass assembly at $z < 1$. These objects are often observed to host a supermassive black hole (SMBH) in their center ([7]). The process of matter accretion into these SMBHs may release a large amount of energy, resulting in Active Galactic Nuclei (AGN). There are two primary modes in which SMBH accretion can occur: the so-called 'quasar mode' and the 'radio mode'. The quasar mode involves a high accretion rate of the SMBH via an optically- thick and geometrically-thin disk, with most of the energy being released in the form of radiation. In a radio mode scenario, the SMBH accretion of gas occurs at a low rate with an optically-thin and geometrically-thick disk configuration, releasing energy in the form of relativistic particles, i.e. radio jets. The latter is typically observed in BCGs [8].

The evolutionary processes of BCGs are still not fully understood, and there are no specific studies comparing the frequency of different types of AGN in BCGs with respect to other types of galaxies (e.g., [9]). The main scientific question guiding my thesis project is to investigate whether the different evolution of BCGs, coupled with their "special" environment, promotes the accretion of SMBHs in their centers compared to other types of galaxies in the local universe, at $z < 0.1$. To address this question, I analyzed a sample of BCGs within the redshift range of z = 0.02-0.1. This sample was derived from the combination of the Sloan Digital Sky Survey Data Release 7 (SDSS DR7 [10]) and the C4 BCGs catalogue produced by

[11, 12]. I utilized the flux measurements of optical emission lines i.e. $H\alpha$, [OIII], $H\beta$, [NII], and [SII] doublets estimated by the Max Planck Institute for Astrophysics and Johns Hopkins University (MPA-JHU) teams using the methods outlined in [13]. This allowed me to conduct a selection of optical AGN through the [NII]- and [SII]- BPT diagnostic diagrams [14]. Additionally, I conducted a cross-matching of the aforementioned catalogs with a dataset obtained from [15], where the spectroscopic sample of the SDSS DR2 was cross-correlated with catalogs of galaxies observed from the National Radio Astronomy Observatory (NRAO) Very Large Array (VLA) Sky Survey (NVSS; [16]) and the Faint Images of the Radio Sky at Twenty centimeters (FIRST) survey [17]. Using this new catalog of BCGs probed with these radio surveys, I was able to select the BCGs that exhibit radio loudness. Following this classification, I finally estimated the fraction of BCGs classified as Optical and Radio Loud AGN. Subsequently, I derived these fractions for a sample of non-BCG selected galaxies using the same procedure employed to obtain the BCG catalog.

These analyses reveal that BCGs exhibit a higher fraction of Optical AGN, in a range of 58% to 74%, compared to the non-BCG sample, which shows a lower percentage $\sim 13\%$, consistent with the results found by [18]. Simultaneously, the analysis of Radio Loud emissions indicates that BCGs are more inclined to host Radio Loud Activity, with a fraction of $\sim 12\%$. This fraction is found to be 20 times higher than the fraction observed in the non-BCG sample of selected galaxies, which is $\sim 0.6\%$.

In conclusion, these results demonstrate that BCGs are more likely to host optical AGN activity and radio-loud emission compared to other types of galaxies. This suggests that their privileged position facilitates frequent accretion of SMBHs in both accretion modes. Previous studies (e.g. [11, 19, 20]) have already shown a prevalence of radio AGN among the BCG population in the local Universe. On the other hand, few studies (e.g., [9, 11]) have attempted to compare the distribution of BCGs in BPT diagrams to that of normal galaxies. The fact that the fraction of AGN is greater for special galaxies is important to understand the nature of these objects. Future studies will aim to test the results obtained with this sample and to understand if this higher fraction is specifically driven by differences in properties between BCGs and non-BCGs, such as mass, star formation rate, metallicity, and kinematics.

Contents

Chapter 1

Introduction

1.1 The Active Galactic Nuclei: Quasar vs. Radio Accretion Modes

Active galaxies constitute a distinctive class characterized by an intensely energetic source at their center, known as an Active Galactic Nucleus (AGN). Since the first observation of an active galaxy in the early 1900s [21], numerous studies have been conducted on this intriguing category of galaxies. To this day, efforts persist in unraveling the nature and role of active galaxies within the broader context of galactic formation and evolution.

Research in this field has demonstrated that the intense radiation must emanate from a compact region, with a spatial dimension not exceeding 100 parsecs. This estimation was derived from the temporal variability observed in some of these sources [22]. Additionally, it has been noted that AGNs exhibit luminosity variations of over 50% within timescales ranging from days to years. Such fluctuations can only be explained if a substantial portion of the emission region is randomly connected. These observations strongly imply that the central component of AGNs is a rapidly accreting Supermassive Black Hole (SMBH).

AGN emissions span the entire electromagnetic spectrum, each wavelength band offers insights into specific components and associated phenomena within AGN [23].

In addition to the central SMBH [7] there is a disk of accreting matter onto it, that emits a significant amounts of ultraviolet (UV) radiation. Above this disk, a cloud of relativistic electrons is believed to be there [24].

This cloud reprocess the UV photons emitted from the disk, re-emitting them at X-ray energy levels. A population of clouds exists in close proximity to the SMBH, that is known as the Broad Line Region (BLR), because the kinematics of these clouds are significantly affected by the gravitational pull of the SMBH, resulting in broader spectral lines. Beyond the BLR, there exists an outer region surrounding the SMBH known as the Narrow Line Region (NLR). In contrast to the BLR, the NLR is characterized by narrower spectral lines, indicating distinct physical conditions and dynamics. Additionally, surrounding the disk, there's a toroidal-shaped volume composed of a mixture of gas and dust, leading to the partial absorption of central radiation. The torus is the main component used from the "Unified Model" [25] to explain the existence of different populations of AGN. According to this model, different AGNs are the same population of objects with specific inclinations to our line-of-sight direction [26].

In particular it is possible to distinguish :

- **Type I:** For these types of AGN, broad emission lines, emitted from the BLR, with typical width in the range of in the range of $\sim 10^3$-10^4 km s^{-1} exhibit a broad component, along with narrow emission lines from the NLR. In this configuration, the observer is situated at a small angle relative to the torus axis, allowing the radiation from circumnuclear regions to remain unobscured along the line of sight.

- **Type II:** In this scenario, the spectrum of the AGN comprises solely narrow emission lines, not exceeding 1200 km s^{-1}, due to the fact that the line of sight intersects the obscuring matter of the torus, obscuring the BLR.

A visual depiction of the Unified Model is shown in Figure 1.1.

The energy released during the accretion process of a SMBH plays a significant role in shaping the evolution of the host galaxy [27]. In this context, the literature often discusses positive and negative feedback mechanisms. Positive feedback occurring when the AGN feedback promotes stellar formation, while negative feedback involves the suppression of star formation, respectively. Feedback from SMBH accretion is capable of heating diffuse gas [28] and depositing heavy elements across the extensive surrounding environment [29], with effects observed at scales exceeding kpc scales. Two

distinct AGN feedback mechanisms have been proposed, each associated with different rates of mass accretion onto the SMBH (e.g. [30, 31]).

- **QSO's Radiative Feedback :** This feedback mode, often referred as quasar mode, consists in a high accretion rate of the SMBH via an optically-thick and geometrically-thin disk, and most of the energy is released in form of radiation.
- **QSO's Radio Feedback :** In this scenario, the SMBH accretion of hotter gas happens with a low rate in a optically-thin and geometrically-thick disk configuration, releasing energy in form of relativistic particles such as Radio Jets.

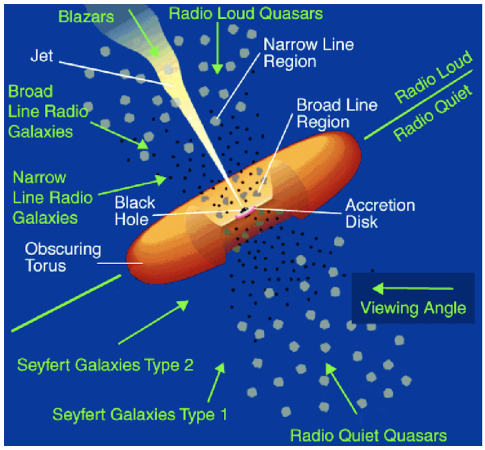

Figure 1.1: The Unified AGN model as proposed in [25], It elucidates AGN taxonomy by considering various viewing angles relative to the torus.

1.2 The Brightest Cluster Galaxies

The Hierarchical Galaxy Formation Model stands as a cornerstone in our understanding of cosmic structure formation, delineating the principal pathways through which galaxies growth their stellar and gas mass assimilating matter from their surroundings [32].

One of the most extreme examples in this context involves the study of Brightest Cluster Galaxies (BCGs), a unique class of galaxies, situated at the center and typically standing out as the most luminous and massive objects within the entire cluster.(e.g. [33]). Considering their environment,

observational studies, have indicated that the evolution of BCGs differs from the normal galactic path [4]. As different studies have shown, BCGs' mass assembly is primarily influenced by dry mergers [5, 6].

The majority of the BCGs are elliptical galaxies, but their properties deviate from established scaling relations for ellipticals. While most BCGs align with the Fundamental Plane, deviations, such as lower velocity dispersions and larger radii than predicted by the Faber–Jackson and Kormendy relations, have been observed (e.g [34]). Recent findings suggest variations in these relations based on galaxy luminosity for all ellipticals. Additionally, BCG surface brightness profiles and radii depend on host cluster properties [35].

BCGs are mainly characterized by Radio Mode accretion of their SMBH, thus exhibiting radio loud emission as well as radio jets. As presented in [11] these relativistic jets of radio emission are also recognized as one of the main explanation of the so called "Cooling flow problem". While Theoretical expectations propose rapid cooling and gas flow toward the center, fostering new star formation, actual observations reveal a much slower cooling process, leading to the discrepancies. The inclusion of radio jets provides a resolution to this issue by infusing energy into the Intracluster Medium (ICM), the hot gas within a galaxy cluster. This injection hinders the rapid cooling and collapse of gas toward the center, deviating from theoretical predictions. However observational studies found that temperature of cluster cores fails to fall below $\sim 30\%$ at large radii resulting in an amount of cooling gas corresponding only to the $\sim 10\%$ expected from the existent cooling flow model. [36]

1.3 Main Scientific Question of the Thesis

In this context, the main scientific question driving this work is to understand **whether the special evolution of BCGs, along with their dense environment, affects the accretion of SMBHs in their centers compared to other types of galaxies in the local universe**.

In particular, this study will present a comparative analysis between two representative samples of BCGs and Non-BCGs to highlight the substantial differences that the cluster environment induces in SMBH accretion.

To address this particular question, I conducted an analysis on a galaxy sample, the Sloan Digital Sky Survey Data Release 7 (SDSS DR7), as outlined in [10], and the C4 BCGs catalogue by Anja Von Der Linden and Best [11]. For these specific BCGs and non-BCGs sample, I utilized the common optical line fluxes ($H\alpha$, [OIII], $H\beta$, [NII], and [SII] doublets) provided by the Max Planck Institute for Astrophysics and Johns Hopkins University team to classify the galaxies hosting an AGN on the basis of the standard optical diagnostic diagram known as BPT [14]. Furthermore, through the cross-match between the aforementioned catalogs with datasets derived from NVSS and FIRST radio surveys, as outlined in [15], I identified BCGs associated with radio loud emission, as an indication of the presence of radio mode SMBH accretion and a potential radio jet.

The analyses and the description of the data will be presented in the next chapter.

Chapter 2

Methods

In this thesis, I analyze a dataset comprising the properties of a sample of galaxies from the Seventh Data Release (DR7) of the Sloan Digital Sky Survey. Covering 11,663 square degrees of imaging data, DR7 offers extensive five-band photometry for 357 million celestial objects [10, 37].

As shown in Fig.2.1, the Legacy imaging footprint is depicted as the extensive contiguous gray area on the left side of the upper panel, complemented by three separated gray stripes visible on the right side.

With completed spectroscopy over 9380 square degrees, including 1.6 million spectra of galaxies, quasars, and stars, the SDSS DR7 dataset serves as the primary catalog for this study. A depiction of the spectroscopic coverage is shown in the lower panel of Fig.2.1 .

I will focus on following physical properties : **Redshift** and **Integrated flux with their relative uncertainties** of the common optical lines (i.e. $H\alpha$, $H\beta$...).

In the context of SDSS DR7, these properties are calculated using an automated procedure of gaussian fitting, applied in two subsequent moments. In the first phase the object is classified and redshift is calculated by fitting at the same moment only the emission lines, while in the second part of the procedure this computation is extended to all lines available. It is important to note that **each** line is **individually fitted as a single Gaussian** on the continuum-subtracted spectrum, with modalities presented by O'Donnell [13]. Information on the Radio classification of the galaxies in this sample is obtained from FIRST and NVSS images from Best et Al. [15].

2.1 Data Description

This thesis presents results obtained through the cross-matching of three distinct celestial catalogues:

- **SDSS DR7 :** Main Catalogue of galaxies [10, 37]
- **C4-BCG :** BCG Catalog [12]
- **Best at Al. :** Survey for RadioLoud identification [15]

2.1.1 SDSS DR7

The Sloan Digital Sky Survey (SDSS) project, is a comprehensive astronomical survey that maps the universe by capturing images, spectra, and photometric data of celestial objects over a large area of the sky, with a spectroscopic footprint area of 9'380 deg^2 and an imaging surface covered of 11'663 deg^2 [10] as shown in Fig.2.1.

Observations have been conducted using a a dedicated wide-field 2.5 m telescope [38] located at Apache Point Observatory (APO) near Sacramento Peak in Southern New Mexico. The telescope employs two distinct instruments, making possible both Imaging and Spectroscopy measures. First measurements are carried out with a wide field imager composed by 24x 2048 × 2048 CCDs on the focal plane [39]. This photometric system comprises five color bands (u, g, r, i, and z) that divide the entire range from the atmospheric UV cutoff at 3000 $\mathring{A}$ to the sensitivity limit of silicon CCDs at 11000 $\mathring{A}$ into five essentially non overlapping passbands.

Spectroscopic measurements are carried out with a pair of multiobject double spectrographs, receiving the light from 640 optical fibers, each of the spectrographs cover a wavelength range from 3800 $\mathring{A}$ to 9200 $\mathring{A}$ with a spectral resolution of $\frac{\lambda}{\Delta\lambda} \approx 2000$. [10]

In this thesis, I work with a dataset of properties estimated by the Max Planck Institute for Astrophysics and Johns Hopkins University (MPA-JHU) team for a total of 927,552 galaxies belonging to the Sloan Digital Sky Survey Data Release 7 (SDSS DR7) [10, 37].

The main Physical Properties of interest for this study are **Redshift** and **Integrated flux with relative uncertainty** for common optical lines (i.e., $H\alpha$, $H\beta$, [N II]6584, [O III]5007, [S II]6731, [S II]6716).

These properties resulted from calculations of two automated spectroscopic pipelines : *spectro2d* and *spectro1d* [40].

These pipeline analyzes combined spectra informations, determining object classifications and initial redshifts. Emission and absorption redshifts are independently measured for each object to avoid biases.

Emission line redshifts are then determined by identifying lines through wavelet transform and performing Gaussian fits. The redshift that I use in this thesis is based on the best-fit model of absorption and emission lines.

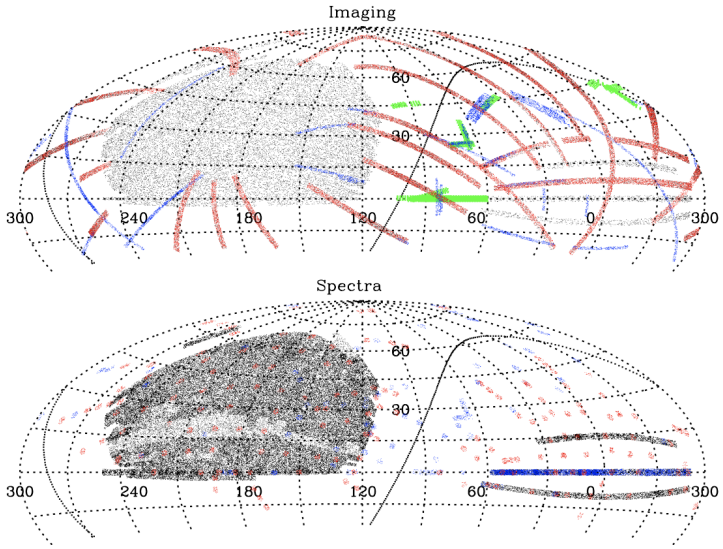

Figure 2.1: Distribution on the sky of the data included in DR7 (upper panel: imaging; lower panel: spectra), shown in an Aitoff equal-area projection in J2000 Equatorial Coordinates. The Galactic plane is the sinuous line that goes through each panel. [10]

2.1.2 C4 BCG Catalogue

The identification of BCGs within the primary galaxy sample, previously described, relies on the BCG catalogue created by A. Von der Linden et al. [11, 12]. This sample is derived from the further analysis of the C4 Galaxy Cluster Catalog, developed by Miller et Al. [41].

The C4 catalog comprises 1106 galaxy clusters identified in the Third Data Release (DR3) of SDSS spanning redshifts from 0.02 to 0.16.

In this context, the work by Von Der Linden et al. [11] is noteworthy, as it builds upon the C4 catalog but introduces improved procedures for

BCG identification and cluster velocity dispersion measurements, ultimately yielding a sample of 625 BCGs.

Despite primarily serving as a cluster catalogue, the original C4 also offered potential BCG candidates by identifying both a *spectroscopic* candidate and a *mean* candidate within each cluster. However, subsequent research conducted by Von Der Linden et al. revealed that approximately 30% of identified clusters missed the true BCG due to fiber collisions in the SDSS spectrometry. To address this issue and to construct a specific BCG sample, Von der Linden's team initially limited the sample by imposing $z \leq 0.1$ in order to ensure that clusters span a large angular extent in comparison to the minimum distance between SDSS spectrometry fibres of ~ 55 arcsec. At this redshift, the magnitude limit in the red band of the spectroscopic sample is approximately $M_r \approx -20$, encompassing an initial sample of 833 clusters. The subsequent selection process involved a specific procedure including the estimation of the virial radius, the selection of the two brightest galaxies within the projection of the mean galaxy, and the application of criteria such as the concentration index and redshift/color compatibility for the final BCG identification. Throughout the computation, several galaxies were lost due to two main structural reasons : initial misclassification of stars and associations with multiple clusters. This led to the rejection of more than 101 clusters, leading to the final sample of 625 elements.

2.1.3 The Radio Catalogue

I also exploit the radio catalog obtained from Best et al., containing 2712 radio sources selected as Radio loud and star-forming [15]. In order to study the fraction of the "BCG" and "non-BCG" samples it has been necessary to cross-match this catalog with that obtained from the match between SDSS and C4 in the previous section. The Authors created this survey from the cross-match of a main spectroscopic galaxy sample and two radio surveys: the National Radio Astronomy Observatories (NRAO) Very Large Array (VLA) Sky Survey (NVSS) [16] and the Faint Images of the Radio Sky at Twenty centimeters (FIRST) [17].

The NVSS was the first radio survey with an angular resolution of 45 arcsec. The FIRST catalogue offers angular resolution of 5 arcsec. Nonetheless, the high angular resolution of FIRST presents its own challenges, as it is

insensitive to extended radio structures and resolves out the extended emission of radio sources. Consequently, the total radio luminosity of sources larger than a few arcseconds is systematically underestimated by FIRST. To address these limitations, a hybrid approach utilizing both NVSS and FIRST surveys has been developed to identify radio sources associated with galaxies in the SDSS spectroscopic sample. This approach capitalizes on the sensitivity of NVSS to large-scale radio structures and the high angular resolution of FIRST to reliably pinpoint the host galaxy.

The obtained radio source sample demonstrated a completeness of 95% and a reliability of 98.9%, upgrading the achievable performance of each individual survey. The sample was subsequently classified into two groups: radio-loud active galactic nuclei (AGN) and galaxies where radio emission is predominantly driven by star formation. Classification was based on galaxies' positions in the plane of 4000 $\mathring{A}$ break strength versus radio luminosity per unit stellar mass, resulting in a dataset of 2,215 radio-loud AGN and 497 star-forming galaxies with radio luminosity exceeding 5 mJy at 1.4 GHz. [15, 42]

2.2 Data Analysis

The initial step of the analysis involved cross-matching the catalog of galaxy properties from the MPA-JHU emission line analysis for the SDSS DR7 with the C4 BCG sample, presented in the previous chapter, in order to identify the BCG candidates. In particular, using coordinates of the galaxies in both these samples, I selected galaxies in the SDSS catalog closest to the individual BCGs in the C4 catalog, within a distance of less than 2 arcseconds (i.e. the PSF of 1.4 arcsec). A distinct catalog was created for galaxies selected as "non-BCG", which were exclusively chosen from within the cross-matched region of these surveys to minimize contamination from BCGs not included in the C4 catalog.

At the end, through this process, i obtained two distinct samples, each containing comprehensive spectral properties for a total of 404 and 389454 galaxies identified as BCG and non-BCG, respectively. In Fig.2.2 I report the distribution of galaxies from SDSS DR7 in grey and the BCGs identified from the crossmatch in red. The black dashed squares show the cross-matched area used to produce the BCG and non-BCG samples.

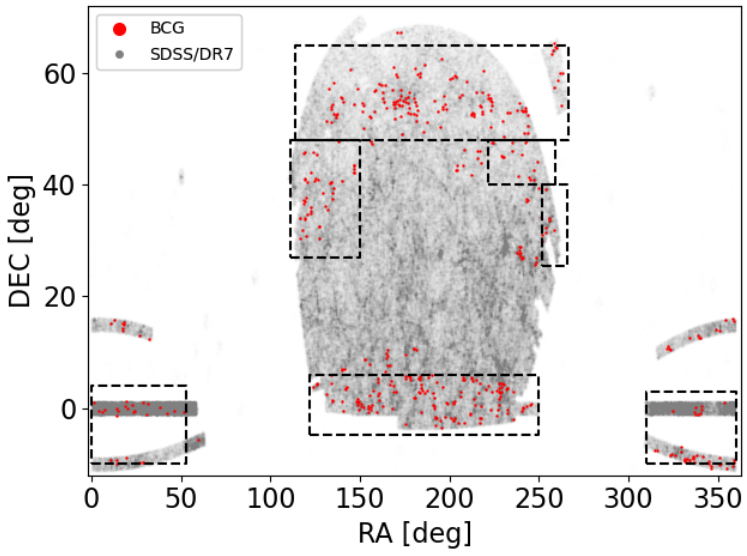

Figure 2.2: Distribution of data on the sky in J2000 Equatorial Coordinates. The grey areas represent galaxies included in the main sample [37], while BCGs identified through crossmatching are highlighted in red. Dashed lines delineate the regions used for constructing the non-BCG sample.

The final step in radio identification involves identifying galaxies exhibiting radio loud emission within both the BCG and non-BCG samples. This additional crossmatching process led to a refinement of the spatial regions, ensuring greater precision in excluding galaxies that may exhibit radio loudness but are not relevant to the radio survey under study.

2.2.1 Optical AGN Identification via BPT Diagram in BCG and non-BCG Samples

In this section, we present an analysis aimed at detecting AGN activity within the galaxies in both the "BCG" and "non-BCG" samples. To do it we use the Baldwin, Phillips & Terlevich (BPT) diagnostic diagram [14]. This analysis is widely performed in literature to classify various types of galaxies based on the ratio of certain optical emission lines emitted from the gas within the host-galaxy, known as the inter-stellar medium (ISM). According to photoionization models, these line ratios are significantly influenced by the properties of the gas and its ionization level. These specific ratios have been carefully chosen to prioritize similar wavelength fractions, minimizing dust attenuation. Specifically, this is developed based on the following ratios: $([OIII]\lambda5007/H\beta), ([NII]\lambda6583/H\alpha), ([SII]\lambda\lambda6716,6731/H\alpha), ([OI]\lambda6300/H\alpha)$.

While the ideal classification incorporates all three primary BPT diagnostics, this study relies on a classification derived solely from the BPT diagrams for [NII] and [SII], based on the plot of $[OIII]\lambda5007/H\beta$ versus $[NII]\lambda6583/H\alpha$ and $[OIII]\lambda5007/H\beta$ versus $[SII]\lambda\lambda6716,6731/H\alpha$, respectively.

According to different photoionization models, demarcation lines can be drawn for the purpose to classify galaxies into different categories [43]. Specifically, galaxies are classified into AGN, Composite, and Star Forming in the BPT-[NII] diagram, and as Seyferts, LINERs, and Star Forming in the BPT-[SII] diagram. I provide an explanation of the nature of the different categories to follow:

- **AGN:** Galaxies dominating the upper-right part of the diagram are characterized by high [NII]/Hα and [OIII]/$H\beta$ ratios suggesting that non-stellar processes play a crucial role in ionization.
- **Composite:** The intermediate region between star-forming and AGN-dominated areas is occupied by galaxies that show a combination of

both star formation and AGN activity. Emission line ratios, including [NII]/Hα and [OIII]/Hβ, fall in intermediate ranges compared to pure star-forming or AGN-dominated regions.

- **Seyferts:** The upper-right portion of the diagram is dominated by galaxies with high [SII]/Hα and [OIII]/Hβ ratios meaning strong non-stellar ionization processes.

- **LINERs (Low-Ionization Nuclear Emission-line Regions):** The intermediate region between star-forming and Seyfert areas is populated by galaxies exhibiting low-ionization emission lines in their nuclei. This suggests a presence of weak AGN activity with low [OIII]/Hβ and intermediate [SII]/Hα ratios.

- **Star-forming :** Galaxies situated in the lower-left region of the diagram are primarily influenced by ongoing star formation. Emission line ratios, such as low [NII]/Hα or [SII]/Hα and [OIII]/Hβ, indicate ionization predominantly driven by massive stars.

The classification via BPT diagnostic diagrams is based on the demarcation functions presented in Kewley et al 2006 [43], that are outlined to follow:

- **BPT-[NII] Demarcation Functions:**

  - Kauffmann+03 Line:

$$\log(\frac{[\mathrm{OIII}]}{\mathrm{H}\beta}) = 0.61/(\log(\frac{[\mathrm{NII}]}{\mathrm{H}\alpha}) - 0.05) + 1.3$$

  - Kewley+01 Line:

$$\log(\frac{[\mathrm{OIII}]}{\mathrm{H}\beta}) = 0.61/(\log(\frac{[\mathrm{NII}]}{\mathrm{H}\alpha}) - 0.47) + 1.19$$

- **BPT-[SII] Demarcation Functions:**

  - Main AGN Line:

$$\log(\frac{[\mathrm{OIII}]}{\mathrm{H}\beta}) = 0.72/(\log(\frac{[\mathrm{SII}]}{\mathrm{H}\alpha}) - 0.32) + 1.30$$

– LINER/Sy2 Line:

$$\log(\frac{[\mathrm{OIII}]}{\mathrm{H}\beta}) = 1.89\log(\frac{[\mathrm{SII}]}{\mathrm{H}\alpha}) + 0.76$$

In the first step, aimed at estimating the fraction of different type of galaxy classification within the BPT diagrams, I operate a further selection of "BCG" and "non-BCG" in order both to include those with all flux emission lines with signal-to-noise ratio larger than three ($SNR > 3$) and to have the BCG and non-BCG sample in the same redshift range, that is $0.02 \leq z \leq 0.1$. The BPT-[NII] and -[SII] diagnostic diagrams for the BCG and non-BCG samples, are reported in Figure 2.3, 2.4, 2.5 2.6, respectively.

Given that the primary aim of this analysis is to quantify the fractions of distinct galaxy types (e.g., HII regions, LINERs, Seyferts, AGNs) within the two subsamples, I employed a robust bootstrap algorithm. For this procedure, I conduct 5000 iterations. In each iteration, I estimate the fraction of galaxies within each region of the BPT diagram by randomly varying the values of the line ratios within their 1σ uncertainties considering a Gaussian probability distribution. After that, I obtain a set of values of the fractions for different populations, of which I derive the mean and standard deviation to estimate the final fractions and relative uncertainties that I present in the next chapter in Table 3.1.

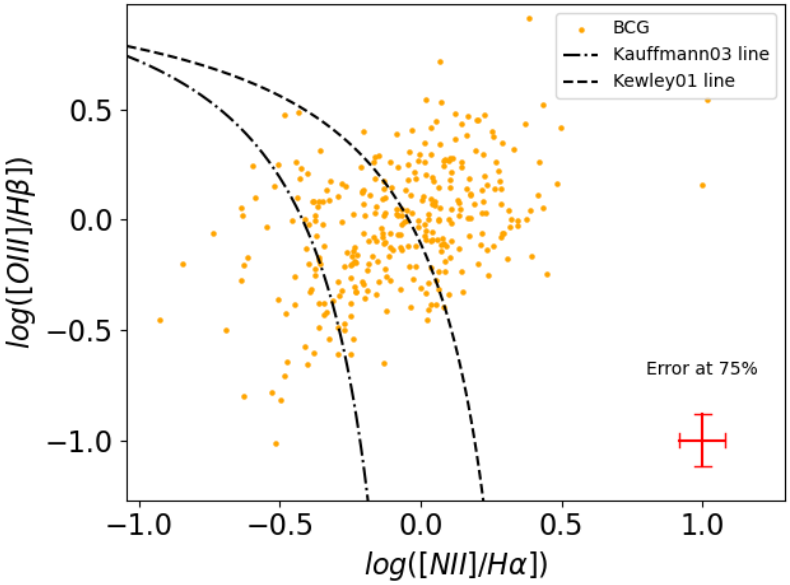

Figure 2.3: BPT diagnostic diagram [NII] for the BCG sample with demarcation lines according to [43]. Additionally, a cross is placed to represent the 75th percentile of the error distribution for all points in the diagram.

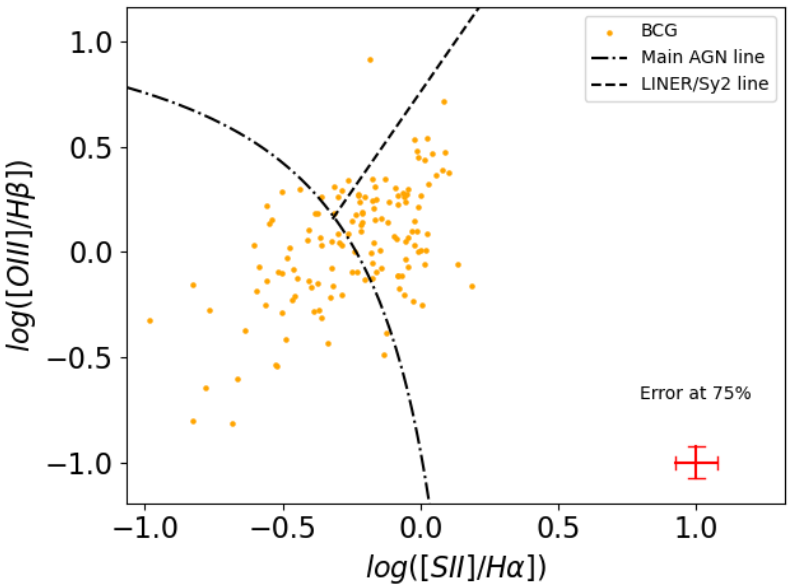

Figure 2.4: BPT diagnostic diagram [SII] for the BCG sample with demarcation lines according to [43]. Additionally, a cross is placed to represent the 75th percentile of the error distribution for all points in the diagram.

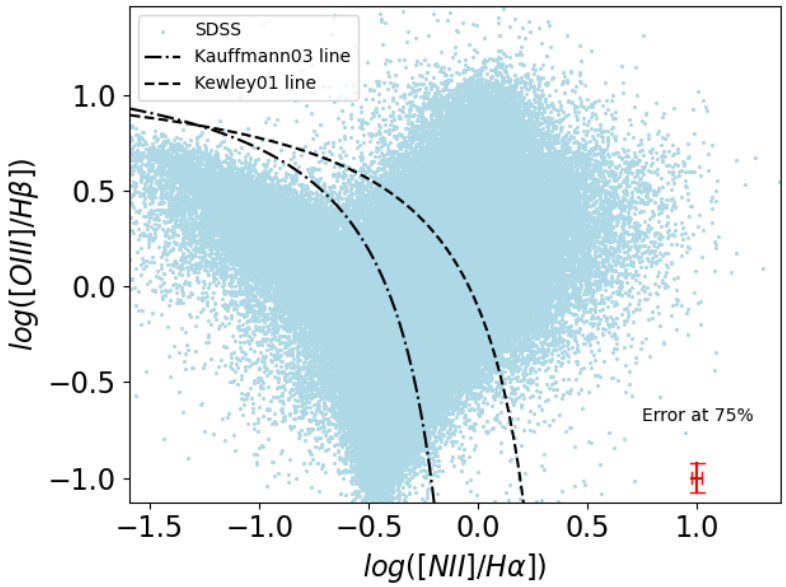

Figure 2.5: BPT diagnostic diagram [NII] for the non-BCG sample with demarcation lines according to [43]. Additionally, a cross is placed to represent the 75th percentile of the error distribution for all points in the diagram.

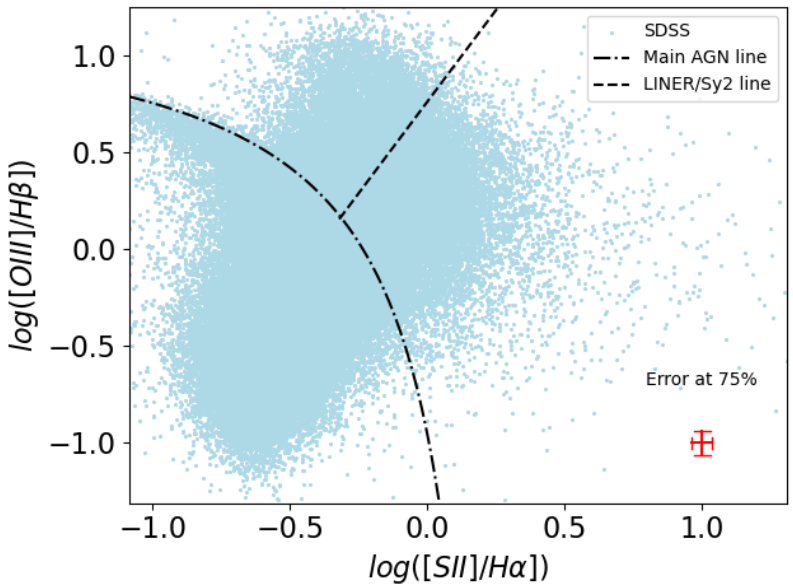

Figure 2.6: BPT diagnostic diagram [SII] for the non-BCG sample with demarcation lines according to [43]. Additionally, a cross is placed to represent the 75th percentile of the error distribution for all points in the diagram.

2.2.2 Radio AGN activity in BCG and non-BCG galaxies

In this analysis I use the catalog from Best et al. [15] based on observations from NVSS and FIRST surveys, to estimate the fraction of BCGs and non-BCGs galaxies exhibiting radio emission due to AGN activity. A crucial step in calculating a representative fraction of Radio Loud objects was to appropriately define the spatial regions for the fraction calculations. To accomplish this, I identified the regions mapped by the radio survey employed. Subsequently, the selection has been delineated in the overlap of the three catalogs employed in this study. It is essential to emphasize that the primary objective is to obtain representative fractions of radio loud activity for the galaxies in both samples. Based on the previously explained details regarding the precision of the Radio survey, galaxies displaying radio loudness were selected from the SDSS dataset within a distance of less than 5 arcseconds, equivalent to the beam size of the radio observations. This process resulted in two distinct samples, each containing both spectral properties and radio loud detections, for a total of 409 and 365,666 galaxies identified as BCG and non-BCG, respectively. In Fig.2.7, I report the refined spatial regions required for determining the radio loud fractions, along with a visual representation of the BCGs and the radio emitters identified through cross-matching the catalogues.

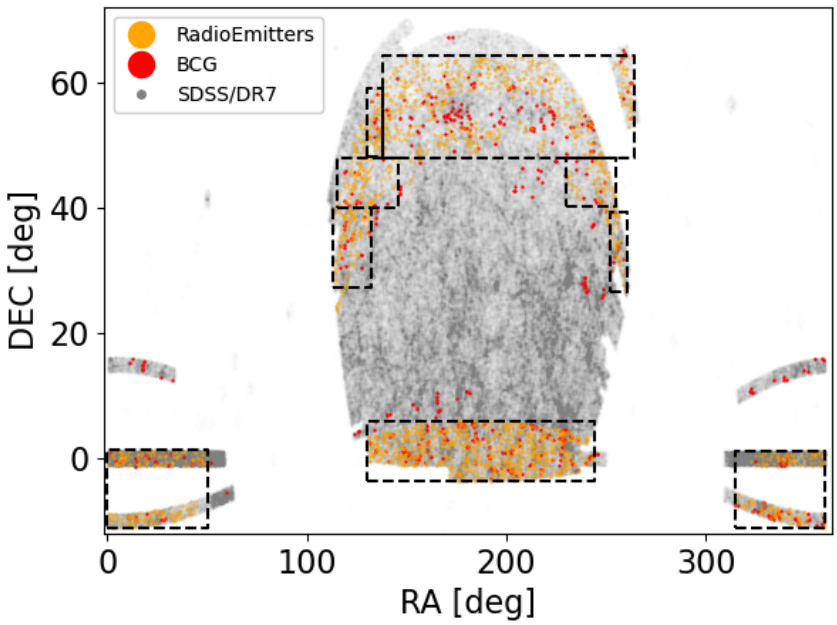

Figure 2.7: Distribution of data on the sky in J2000 Equatorial Coordinates. The grey areas depict galaxies included in the main sample [37], while BCGs identified through crossmatching are highlighted in red. Sources of radio emission found by Best et al. [15] are shown in orange. Dashed lines delineate the sky regions where the calculation of Radio Loud AGN fractions has been defined.

Chapter 3

Results

Table 3.1 shows the fractions estimated from the analysis of the BPT diagnostic diagrams for the two samples collecting galaxies selected as BCG and non-BCG, according to the selection on signal-to-noise ratio (SNR) greater than 3 and aligning non-BCGs to the same redshift range as BCGs. This filtering resulted in a set of 149 and 78 galaxies, respectively, for the BPT-[NII] and BPT-[SII] diagrams in the BCG sample. In the same context, there were 98,571 and 88,867 galaxies for the non-BCG sample. To evaluate AGN activity, particularly in the BPT-[SII] diagnostic diagram, the combination of the Seyfert and LINER categories allows a further estimation of the maximum percentage. Analyzing the results presented in Table 3.1 , the fraction of AGN in the BCGs sample range from 58% to 74%. In the corresponding context, non-BCGs exhibit percentages in the range of 12% to 13%. These values are consistent with the findings of [18], even if the results they report is derived from a larger sample that includes BCGs and sources with a SNR also lower than 3. This calculations indeed show that BCGs show a greater optical AGN fraction, with respect to non BCGs. A further analysis was also implemented by dividing the BCG sample into four bins with the same number of elements and calculating the AGN fractions for both samples in relation to these bins. Results of the latter, depicted in Fig.3.1, suggest that although the AGN fraction for non-BCGs shows a slight increase within the redshift range of BCGs (i.e., $0.02 \leq z \leq 0.1$), the corresponding percentages for BCGs remain constant at a value of 65/70%, as depicted in Fig.3.1. Such an increase could not be detected with these calculations in the BCG sample, due to both smaller statistics and a broader dispersion of errors, but these results cannot exclude it. In this context, for future developments, it

would be interesting to analyze the reasons behind the broader dispersion of errors for the fraction of non-BCGs at lower redshift.

Lastly, the analysis dedicated for detecting the BCGs and non-BCGs associated with radio loud emission indicates that BCGs are more likely to host radio luminosity exceeding 5mJy at 1.4 GHz, with a fraction of 12%. This value is 20 times higher than the fraction found for the non-BCG subsample of galaxies within the selected regions, as discussed earlier, corresponding to 0.6%.

Diagram	Classification	non-BCG	BCG
[NII]	AGNs	12.04 ± 0.03 %	58.0 ± 1.8 %
	Composites	17.49 ± 0.05 %	34.7 ± 2.2 %
	SFGs	70.47 ± 0.03 %	7.3 ± 0.2 %
[SII]	Seyferts	4.22 ± 0.03 %	6.6 ± 1.7 %
	LINERs	9.03 ± 0.04 %	67.6 ± 2.5 %
	SFGs	86.75 ± 0.04 %	25.9 ± 2.1 %

Table 3.1: Results of the classification using BPT diagnostic diagrams, following the criteria established by Kewley et al. [43]. The samples were refined by requiring a signal-to-noise ratio (SNR) greater than 3 and aligning non-BCGs within the same redshift range as BCGs. The results are presented as percentages for each population.

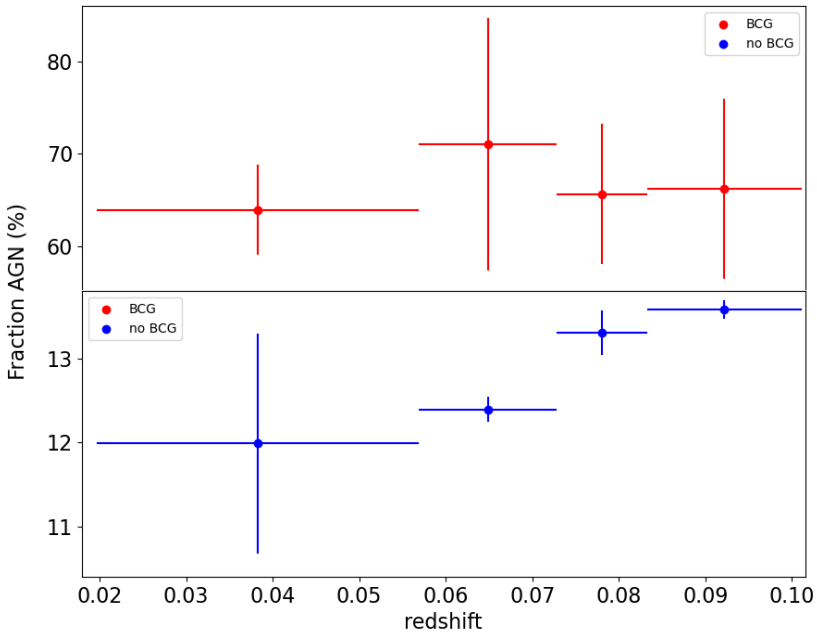

Figure 3.1: Visual representation illustrating the stability of AGN activity in BCGs across redshifts, contrasted with a slight increase observed in the non-BCG sample. Fractions were calculated by including AGN galaxies in the BPT [NII] diagnostic diagram and Seyferts together with LINERs in the BPT [SII] diagnostic diagram. The four redshift bins are uniformly defined to maintain the same BCG statistics within each bin. The samples underwent further refinement by imposing a signal-to-noise ratio (SNR) threshold greater than 3 and aligning non-BCGs within the identical redshift range as BCGs.

Summary and Conclusions

The evolutionary processes of BCGs are still not fully understood, and there are just few studies comparing the frequency of different types of AGN in BCGs based on BPT diagram analysis (e.g., [9]).

The central inquiry driving this thesis project is: *Does the unique evolutionary path of BCGs, shaped by their distinctive environmental conditions, contribute to heightened SMBH accretion at their cores compared to other galaxy types in the local universe?*

To tackle this scientific inquiry, this study conducts a comparative analysis on samples of Brightest Cluster Galaxies (BCGs) and non-BCGs. The samples are derived through the cross-matching of three distinct catalogs, encompassing a comprehensive sample of galaxies [10], catalogs of selected BCGs [12], and radio-loud sources [15] associated to these galaxies, in a specific overlapped area shown in Fig.2.7.

Using the spectroscopic properties of the optical lines derived from MPA-JHU team in the context of SDSS DR7 [10, 37], I estimated the fraction of Optical AGN and radio emission from AGN activity, in samples of BCGs and non-BCGs and I found following results. Assuming the effectiveness of the BPT diagnostic diagrams classification I determined that, within a sample refined with a signal-to-noise ratio greater than 3, approximately a range from 58% to 74% of BCGs host an AGN. Compared with non-BCGs in the same redshift range, with the same requirement in SNR, i detected a range of 12% to 13%. The higher AGN activity observed in the BCG galaxies, in a range of 4x to 6x times higher, as derived from the BPT analyses contrasts with some studies that have found a typically higher AGN fraction in the field compared to clusters (i.e. [44]). On the other hand, it agrees with other studies, also based on BPT diagram analyses (i.e. [45]). The fact that BCGs exhibit more common AGN activity can be attributed to the large amount of hot gas, typically detected as X-rays in galaxy clusters'

ICM , which cools and falls into the BCG, fueling both galaxy growth and the supermassive black hole in previous stages [45].

The fraction of BCGs that exhibit Radio Loud emission is 20x higher than the value resulted for non-BCGs galaxies. This evidence may suggest that the unique environmental conditions within the cluster play a crucial role in shaping the accretion mode of SMBH at the center of the BCG, as well as the subsequent AGN feedback, as widely shown in literature (i.e.[46, 47]). The same conclusion can be achieved by looking at the results showing an higher percentage of LINERs in the BPT-[SII] diagram. Indeed, LINERs are objects in which the low-ionization nuclear emission lines such as [NII] and [SII] are excited. Some authors (i.e. [48]) suggest that these high excitation are a consequence of shock-induced gas interactions through radio jets.

The scope of this thesis could be extended by delving into the intrinsic properties of BCGs that might be intricately associated with the presence of an AGN or radio loud emissions. This entails a comprehensive exploration of data provided by the MPA-JHU to gain insights into the intrinsic characteristics of BCG populations more prone to hosting AGN activities, including factors such as mass, star formation rate (SFR), and redshift. To accomplish this, a logical progression would involve a more in-depth examination of the two distinct samples already established – one comprising BCGs and the other non-BCGs.

Bibliography

[1] A. Sandage and Kristian. The extension of the Hubble diagram. I. New redshifts and BVR photometry of remote cluster galaxies, and an improved richness correction. *The Astrophysical Journal*, 205:688–695, May 1976. doi: 10.1086/154324.

[2] Anja von der Linden and Wild. Star formation and AGN activity in SDSS cluster galaxies. *Monthly Notices of the Royal Astronomical Society*, 404(3):1231–1246, May 2010. doi: 10.1111/j.1365-2966.2010.16375.x.

[3] Danièl N. Groenewald and Skelton. The close pair fraction of BCGs since z = 0.5: major mergers dominate recent BCG stellar mass growth. *Monthly Notices of the Royal Astronomical Society*, 467(4):4101–4117, June 2017. doi: 10.1093/mnras/stx340.

[4] A. Travascio and Bongiorno. Multiple AGN activity during the BCG assembly of XDCPJ0044.0-2033 at z $\sim$ 1.6. *Monthly Notices of the Royal Astronomical Society*, 498 (2):2719–2733, October 2020. doi: 10.1093/mnras/staa2495.

[5] Gabriella De Lucia and Jérémy Blaizot. The hierarchical formation of the brightest cluster galaxies. *Monthly Notices of the Royal Astronomical Society*, 375(1):2–14, February 2007. doi: 10.1111/j.1365-2966.2006.11287.x.

[6] Kevin C. Cooke and Kartaltepe. Stellar Mass Growth of Brightest Cluster Galaxy Progenitors in COSMOS Since z $\sim$ 3. *The Astrophysical Journal*, 881(2):150, August 2019. doi: 10.3847/1538-4357/ab30c9.

[7] D. A. Rafferty and McNamara. The Feedback-regulated Growth of Black Holes and Bulges through Gas Accretion and Starbursts in Cluster Central Dominant Galaxies. *The Astrophysical Journal*, 652(1):216–231, November 2006. doi: 10.1086/507672.

[8] John P. Stott and Hickox. The XMM Cluster Survey: the interplay between the brightest cluster galaxy and the intracluster medium via AGN feedback. *Monthly Notices of the Royal Astronomical Society*, 422(3):2213–2229, May 2012. doi: 10.1111/j.1365-2966.2012.20764.x.

[9] S. Fisek and Alis. AGN Activity in Brigtest Cluster Galaxies (BCGs). *Communications of the Byurakan Astrophysical Observatory*, 66(2):153–158, December 2019. doi: 10.52526/25792776-2019.66.2-153.

[10] Kevork N. Abazajian and Adelman-McCarthy. The Seventh Data Release of the Sloan Digital Sky Survey. *Astrophysical Journal Supplement Series*, 182(2):543–558, June 2009. doi: 10.1088/0067-0049/182/2/543.

[11] Anja Von Der Linden and Best. How special are brightest group and cluster galaxies? *Monthly Notices of the Royal Astronomical Society*, 379(3):867–893, August 2007. doi: 10.1111/j.1365-2966.2007.11940.x.

[12] A. von der Linden and Best. VizieR Online Data Catalog: BCG C4 cluster catalog (von der Linden+, 2007). VizieR On-line Data Catalog: J/MNRAS/379/867. Originally published in: 2007MNRAS.379..867V, July 2009.

[13] James E. O'Donnell. R v-dependent Optical and Near-Ultraviolet Extinction. *The Astrophysical Journal*, 422:158, February 1994. doi: 10.1086/173713.

[14] J. A. Baldwin, M. M. Phillips, and R. Terlevich. Classification parameters for the emission-line spectra of extragalactic objects. *Publications of the Astronomical Society of the Pacific*, 93:5–19, February 1981. doi: 10.1086/130766.

[15] P. N. Best, G. Kauffmann, T. M. Heckman, and Ž. Ivezić. A sample of radio-loud active galactic nuclei in the Sloan Digital Sky Survey. *Monthly Notices of the Royal Astronomical Society*, 362(1):9–24, September 2005. doi: 10.1111/j.1365-2966.2005.09283.x.

[16] J. J. Condon and Cotton. The NRAO VLA Sky Survey. *The Astronomical Journal*, 115(5): 1693–1716, May 1998. doi: 10.1086/300337.

[17] Robert H. Becker and White. The FIRST Survey: Faint Images of the Radio Sky at Twenty Centimeters. *The Astrophysical Journal*, 450:559, September 1995. doi: 10.1086/176166.

[18] M. Vitale and Zuther. Classifying radio emitters from the Sloan Digital Sky Survey. Spectroscopy and diagnostics. *Astronomy & Astrophysics*, 546:A17, October 2012. doi: 10.1051/0004-6361/201219290.

[19] Z. S. Yuan, J. L. Han, and Z. L. Wen. Radio luminosity function of brightest cluster galaxies. *Monthly Notices of the Royal Astronomical Society*, 460(4):3669–3678, August 2016. doi: 10.1093/mnras/stw1125.

[20] P. Oliva-Altamirano and Brough. Galaxy And Mass Assembly (GAMA): testing galaxy formation models through the most massive galaxies in the Universe. *Monthly Notices of the Royal Astronomical Society*, 440(1):762–775, May 2014. doi: 10.1093/mnras/stu277.

[21] Gregory A. Shields. A brief history of active galactic nuclei. *Publications of the Astronomical Society of the Pacific*, 111(760):661, jun 1999. doi: 10.1086/316378. URL `https://dx.doi.org/10.1086/316378`.

[22] L. Woltjer. Emission Nuclei in Galaxies. *The Astrophysical Journal*, 130:38, July 1959. doi: 10.1086/146694.

[23] Paolo Padovani. On the two main classes of active galactic nuclei. *Nature Astronomy*, 1: 0194, August 2017. doi: 10.1038/s41550-017-0194.

[24] M. Kishimoto, R. Antonucci, C. Boisson, and O. Blaes. Revealing AGN by Polarimetry. In A. Adamson, C. Aspin, C. Davis, and T. Fujiyoshi, editors, *Astronomical Polarimetry: Current Status and Future Directions*, volume 343 of *Astronomical Society of the Pacific Conference Series*, page 435, December 2005. doi: 10.48550/arXiv.astro-ph/0408106.

[25] C. Megan Urry and Paolo Padovani. Unified Schemes for Radio-Loud Active Galactic Nuclei. *Publications of the Astronomical Society of the Pacific*, 107:803, September 1995. doi: 10.1086/133630.

[26] Robert Antonucci. Unified models for active galactic nuclei and quasars. *Annual Review of Astronomy and Astrophysics*, 31:473–521, January 1993. doi: 10.1146/annurev.aa.31.090193.002353.

[27] V. A. Masoura and Mountrichas. Relation between AGN type and host galaxy properties. *Astronomy & Astrophysics*, 646:A167, February 2021. doi: 10.1051/0004-6361/202039238.

[28] Tiziana Di Matteo and Springel. Energy input from quasars regulates the growth and activity of black holes and their host galaxies. *Nature*, 433(7026):604–607, February 2005. doi: 10.1038/nature03335.

[29] Karl Gebhardt and Bender. A Relationship between Nuclear Black Hole Mass and Galaxy Velocity Dispersion. *Astrophysical Journal Letters*, 539(1):L13–L16, August 2000. doi: 10.1086/312840.

[30] A. C. Fabian. Observational Evidence of Active Galactic Nuclei Feedback. *Annual Review of Astronomy and Astrophysics*, 50:455–489, September 2012. doi: 10.1146/annurev-astro-081811-125521.

[31] C. M. Harrison. Impact of supermassive black hole growth on star formation. *Nature Astronomy*, 1:0165, July 2017. doi: 10.1038/s41550-017-0165.

[32] S. Cole, A. Aragon-Salamanca, C. S. Frenk, J. F. Navarro, and S. E. Zepf. A recipe for galaxy formation. *Monthly Notices of the Royal Astronomical Society*, 271:781–806, December 1994. doi: 10.1093/mnras/271.4.781.

[33] Z. L. Wen and J. L. Han. Dependence of the bright end of composite galaxy luminosity functions on cluster dynamical states. *Monthly Notices of the Royal Astronomical Society*, 448(1):2–8, March 2015. doi: 10.1093/mnras/stu2722.

[34] William R. Oegerle and John G. Hoessel. Fundamental Parameters of Brightest Cluster Galaxies. *The Astrophysical Journal*, 375:15, July 1991. doi: 10.1086/170165.

[35] S. Brough, C. A. Collins, D. J. Burke, P. D. Lynam, and R. G. Mann. Environmental dependence of the structure of brightest cluster galaxies. *Monthly Notices of the Royal Astronomical Society*, 364(4):1354–1362, December 2005. doi: 10.1111/j.1365-2966.2005.09679.x.

[36] L. P. David, P. E. J. Nulsen, B. R. McNamara, W. Forman, C. Jones, T. Ponman, B. Robertson, and M. Wise. A high-resolution study of the hydra a cluster with chandra: Comparison of the core mass distribution with theoretical predictions and evidence for feedback in the cooling flow. *The Astrophysical Journal*, 557(2):546, aug 2001. doi: 10.1086/322250. URL `https://dx.doi.org/10.1086/322250`.

[37] Max-Planck-Institut für Astrophysik. Sdss data release 7, s.d. URL `https://wwwmpa.mpa-garching.mpg.de/SDSS/DR7/`.

[38] Gunn. The 2.5 m Telescope of the Sloan Digital Sky Survey. *The Astronomical Journal*, 131 (4):2332–2359, April 2006. doi: 10.1086/500975.

[39] Gunn. The Sloan Digital Sky Survey Photometric Camera. *The Astronomical Journal*, 116 (6):3040–3081, December 1998. doi: 10.1086/300645.

[40] Stoughton. Sloan Digital Sky Survey: Early Data Release. *The Astronomical Journal*, 123 (1):485–548, January 2002. doi: 10.1086/324741.

[41] Christopher J. Miller and Nichol. The C4 Clustering Algorithm: Clusters of Galaxies in the Sloan Digital Sky Survey. *The Astronomical Journal*, 130(3):968–1001, September 2005. doi: 10.1086/431357.

[42] P. N. Best and Kauffmann. The host galaxies of radio-loud active galactic nuclei: mass dependences, gas cooling and active galactic nuclei feedback. *Monthly Notices of the Royal Astronomical Society*, 362(1):25–40, 09 2005. ISSN 0035-8711. doi: 10.1111/j.1365-2966.2005.09192.x. URL https://doi.org/10.1111/j.1365-2966.2005.09192.x.

[43] Lisa J. Kewley and Groves. The host galaxies and classification of active galactic nuclei. *Monthly Notices of the Royal Astronomical Society*, 372(3):961–976, November 2006. doi: 10.1111/j.1365-2966.2006.10859.x.

[44] P. A. A. Lopes and Ribeiro. NoSOCS in SDSS - VI. The environmental dependence of AGN in clusters and field in the local Universe. *Monthly Notices of the Royal Astronomical Society*, 472(1):409–418, November 2017. doi: 10.1093/mnras/stx2046.

[45] H. S. Hwang, C. Park, D. Elbaz, and Y. Y. Choi. Activity in galactic nuclei of cluster and field galaxies in the local universe. *Astronomy & Astrophysics*, 538:A15, February 2012. doi: 10.1051/0004-6361/201117351.

[46] H. Nagai and Onishi. The ALMA Discovery of the Rotating Disk and Fast Outflow of Cold Molecular Gas in NGC 1275. *The Astrophysical Journal*, 883(2):193, October 2019. doi: 10.3847/1538-4357/ab3e6e.

[47] B. I. Ciocan, B. L. Ziegler, M. Verdugo, P. Papaderos, K. Fogarty, M. Donahue, and M. Postman. The VLT-MUSE and ALMA view of the MACS 1931.8-2635 brightest cluster galaxy. *Astronomy & Astrophysics*, 649:A23, May 2021. doi: 10.1051/0004-6361/202040010.

[48] G. Fabbiano and A. Paggi. Jet–ism interaction in ngc 1167/b2 0258+35, an liner with an agn past. *The Astrophysical Journal*, 938(2):105, oct 2022. doi: 10.3847/1538-4357/ac8ff8. URL https://dx.doi.org/10.3847/1538-4357/ac8ff8.